Electrolytic deposition of reactive element thin films on Crofer 22 APU and evaluation of the resulting high-temperature corrosion protection properties at 700 °C–900 °C

Bartłomiej Lemieszek [a],[*], Justyna Ignaczak [a], Bartosz Kamecki [a], Jakub Karczewski [b], Mogens Bjerg Mogensen [c], Sebastian Molin [a], Piotr Jasiński [a]

[a] Advanced Materials Centre, Faculty of Electronics, Telecommunications and Informatics, Gdańsk University of Technology, Ul. G. Narutowicza 11/12, 80-233 Gdańsk, Poland
[b] Advanced Materials Centre, Faculty of Applied Physics and Mathematics, Gdańsk University of Technology, Ul. G. Narutowicza 11/12, 80-233 Gdańsk, Poland
[c] Department of Energy Conversion and Storage Electrochemistry, Technical University of Denmark, Fysikvej, Building 310, 2800 Kgs. Lyngby, Denmark

HIGHLIGHTS

- New technique of obtaining thin ceramic layers - electrolytic technique.
- Electrolytic deposition of cerium, gadolinium, lanthanum and yttrium oxide layers.
- Thin ceramic layers, on the order of tens of nanometers.
- Reduction of the thermogravimetric weight gain of samples covered with a ceramic layer.
- Electrical measurements showed that the surface-modified samples had lower resistance than the uncoated sample.

ARTICLE INFO

ABSTRACT

This article presents electrolytic deposition of thin Rare Earth (RE) coatings on Crofer 22 APU stainless steel substrates for high temperature applications, such as interconnects in solid oxide cell stacks. The deposition of coatings based on yttrium-, gadolinium-, lanthanum-, and cerium nitrates is discussed. The high temperature corrosion properties of surface-modified steels were examined using thermogravimetry and electrical resistivity measurements. Coatings and oxide microstructures were examined by XRD and SEM of surfaces and cross-sections. The results showed that the use of the RE element oxide layers reduced the growth of oxide scale, as evidenced by lower weight gain. The layers based on Y- and Gd-oxides showed the best corrosion protection properties. The electrical measurements showed that the surface-modified samples had lower resistance than the uncoated sample.

* Corresponding author.
E-mail address: bartlomiej.lemieszek@pg.edu.pl (B. Lemieszek).

Please cite this article as: Lemieszek B et al., Electrolytic deposition of reactive element thin films on Crofer 22 APU and evaluation of the resulting high-temperature corrosion protection properties at 700 °C–900 °C, International Journal of Hydrogen Energy, https://doi.org/10.1016/j.ijhydene.2022.07.220

Introduction

High-temperature corrosion of stainless steel interconnects is one of the main undesirable phenomena of solid oxide cells, limiting their long-term operation [1–3]. Current generation anode-supported Solid Oxide Cells (SOCs) operate at the 600–900 °C temperature range and therefore, surface oxide scale growth is inevitable during exposure of iron-chromium alloys at these temperatures. Due to the low electrical conductivity of the oxide, its growth results in an increase in the electrical resistance across the interconnects, leading to a decrease in the power output of the stack. The increase in resistance and deterioration of physical properties due to corrosion spurred the development of protective layers [4–6]. One type of protective coatings is thick and dense spinel layers that block chromium evaporation. These are mostly based on cobalt or cobalt-manganese oxides [7–10]. Our group has so far extensively studied thick Mn−Co oxide spinel-based coatings for the reduction of Cr-evaporation [11,12]. Another type of coating is very thin Rare Earth elements-based (RE) oxide coatings applied to decrease the rate of corrosion, e.g., cerium-, gadolinium-, lanthanum-, and yttrium oxide [13–17]. These two types of coatings can be combined to obtain synergistic effects [18,19]. The use of even very low RE oxide thickness (~10 nm) coatings is very beneficial in decreasing scale thickness [20,21].

Among the many ceramic deposition methods, the electrolytic technique seems well suited for the deposition of RE oxide thin layers on steel interconnects [22]. In comparison to the electrophoretic deposition process, where solid particles are deposited, the electrolytic method utilises metal salts (e.g. nitrates, chlorides) and solvents (ethanol or water) which, by electrochemical reaction, form deposits on the working electrode [23]. The thickness of the deposits can be controlled by the deposition voltage, time, and concentration of the solution. This method and similar cost-effective techniques have been previously used for the deposition of ceramic coatings in order to improve corrosion protection of steel at high temperature. Some works refer to coating process only, while some include also corrosion tests. Molin et al. presented results of the electrolytic deposition of a Y-based layer from a 0.05 M ethanol solution of yttrium nitrate together with the results of corrosion investigation. The corrosion rate of the yttria−coated Crofer 22 APU sheets at 750 °C was 20 times lower than that of uncoated samples [22]. Zhitomirsky et al. showed the results of coating nickel with the layer of yttrium oxide using precursor consisting of 0.02 M aqueous yttrium nitrate solution mixed with poly (diallyldimethylammonium chloride). During the process of cathodic electrodeposition at the current density of 10 mA cm-2, the layer of about 0.2 μm was obtained [24]. In another work, Zhitomirsky et al. proposed the deposition of the cerium oxide layer by electrolytic technique from 0.01 M cerium chloride solution dissolved in a 19:1 ethanol: water mixture. The deposition at the current density of 10 mA cm^{-2} resulted in the cerium oxide layer thickness of ~0.2−0.3 μm [25]. Yang et al. deposited 0.1−0.3 μm thick layer of cerium oxide using a solution consisting of 5 mM cerium chloride [26]. Mazur et al. proposed coating ferritic steel intended for interconnectors with gadolinium oxide nanoparticles using the electrolytic and immersion techniques. The obtained results indicate a reduction of oxidation rate of about 10 times at 700 °C [27]. Yoon et al. coated steel using the dip-coating technique, which allowed depositing 200−210 nm thick layers of lanthanum oxide. After the 500-h oxidation process at 700 °C, the presence of lanthanum-chromium and manganese-chromium spinels on the sample surface was proven [28]. Saeidpour et al. coated Crofer 22 APU steel with a composite of metallic cobalt and yttrium oxide using the electroplating method. After 500 h at 800 °C, weight gain was much higher for the coated samples than for uncoated one. However, the oxidation rate was greatly reduced, and the coated samples would perform much better in time. The initial greater weight gain was due to the rapid oxidation of cobalt [29]. As presented, RE oxides may be deposited by the cost-effective techniques and usually these layers lower the oxidation rate of the steel, however thorough corrosion protection studies of RE oxides still should be carried out.

This work is an investigation of promising thin RE oxide layers fabricated by electrodeposition. The results of the fabrication of thin ceramic films based on cerium-, yttrium-, gadolinium-, and lanthanum oxides and their effects on the resulting high temperature corrosion properties relevant for solid oxide cells are presented. The surface-modified samples were studied by thermogravimetry, electrical conductivity measurements, and post-mortem analyses (microscopy, diffractometry).

Experimental procedures

Commercial hydrated metal salts: $Gd(NO_3)_3 \cdot 6H_2O$ (Sigma Aldrich 99.9% purity, Saint Louis, United States of America), $Y(NO_3)_3 \cdot 6H_2O$ (Sigma Aldrich 99% pure, Saint Louis, United States of America), $Ce(NO_3)_3 \cdot 6H_2O$ (Honeywell Fluka, North Carolina, United States of America), and $La(NO_3)_3 \cdot 6H_2O$ (Sigma Aldrich 99.99%, Saint Louis United States of America) were used for the preparation of solutions in ethyl alcohol (Sigma Aldrich 99.8%, Saint Louis, United States of America) with a cation concentration of 2 mM. The solution was semi-transparent without visible precipitation even after several months of shelf life. The specific conductivity of electrolytic solutions was determined from impedance spectra obtained by 2-probe measurement with 100 mV amplitude in the range from 100 kHz to 1 Hz. For conductivity calculations, 1 mM and 0.1 M KCl were used as reference solutions.

A 0.3 mm thick sheet of Crofer 22 APU steel (VDM Metals, Verdohl, Germany) was cut into 1.5 × 1.5 cm plates to be used as the substrates for RE electrodeposition. A small hole (3 mm in diameter) was punched in the top part of the samples so they could be suspended on an alumina rod for corrosion exposure. The edges of plates were smoothed out in order to remove visible flexures using a polishing machine with wet 1200 grit paper. Before applying the RE coatings, the plates were thoroughly cleaned in acetone (POCH, Gliwice, Poland) in an ultrasonic bath. The cleaned and dried plates were crocodile clips connected as the working electrode (cathode) in a two-electrode electrolytic deposition system. The counter electrode (anode) was an oversized Crofer 22 APU steel sheet and was placed symmetrically on both sides of the working

electrode (active geometrical surface area of about 50 cm^2). The distance between the working electrode and the counter electrodes was ~1.5 cm 3 samples were made for each RE-oxide, and each sample was weighed three times. Each sample was gently air dried before being annealed at 400 °C. Each operation was performed with extreme care to ensure that the layers were undamaged. A sketch of the deposition setup is presented in Fig. 1.

A voltage of 40 V was applied between the electrodes as in Ref. [19] using a programmable power supply (Delta Elektronika Power Supply SM 300−5, Zierikzee, The Netherlands). Current measurements were recorded using the ammeter (Sanwa PC500A, Sanwa Electric Instrument Co., Ibaraki, Japan). The optimised deposition time for each of the solutions was deduced from the preliminary tests (not reported here). After application of the RE layer, each of the samples was air-dried and heated to a temperature of about 400 °C for complete conversion of the deposited layers to oxides and the decomposition of residual nitrates. This process has been studied and described in the literature [30−32].

To determine corrosion kinetics, the thermogravimetry (weight changes) method was used. Oxidation tests were performed in a chamber furnace (Kittec SQ11, Vranovice-Kelčice, Czech Republic) in stagnant air. The oxidation tests were carried out in a cyclic manner in two stages. The first "pre-evaluation" was based on a relatively short time (250 h with weight measurements every 50 h) at three different temperatures (700 °C, 800 °C, and 900 °C). The second step, "long-term" corrosion study, was carried out for a total of 2000 h at 700 °C with weight gain measurements every 250 h. The weight gain measurements were performed on a balance with an accuracy of 10^{-6} g (Radwag XA 6/21.4Y.M.A.B PLUS, Radom, Poland).

The microstructure of the Crofer 22 APU steel samples was analysed by X-ray diffraction (XRD) using a Bruker D2Phaser (Bruker AXS, Mannheim, Germany) diffractometer with a Lynxeye XE-T detector with CuKα radiation (k = 0.15406 nm). Post-mortem studies in the form of surface and cross-section analyses were performed using a scanning electron microscope with an integrated energy dispersive X-ray (EDS) analyser (Thermo Fischer Phenom XL, Waltham, United States of America).

Electrical resistance measurements were performed in a cross-scale configuration (across Pt/oxide/steel/oxide/Pt). The platinum electrodes (with an area of 0.5 cm^2) were brush-painted on the two sides of the steel, dried and heated to 700 °C for 2 h. The electrical resistance measurement was carried out in a four-electrode system using an impedance analyser (Gamry Interface 1000E, Warminster, PA, United States). The measurement was performed at a frequency of 1 Hz (the imaginary part of the impedance was negligible) with an amplitude of 5 mV. The sample was heated to 700 °C and then cooled to 300 °C while the resistance was measured. The maximum current flowing through the sample was limited to 5 mA cm^{-2}.

Results and discussion

The results section is organised as follows: first, the results related to the deposition process of the RE coatings with different thicknesses are presented. Then an accelerated oxidation screening test of the differently coated samples is shown. Based on the accelerated test, the most promising RE coating thickness was selected. Short-term (250 h at 700/800/900 °C) and long-term oxidation studies are conducted on the selected samples. Finally, post-mortem analyses are performed to describe the microstructures of the samples.

Preparation of the layers

The preparation of the layers was started by analysing the solution conductivity and electrical charge density measurements during the electrodeposition process. Measurements on the solutions of Ce-, La-, Gd-, and Y-nitrates showed specific conductivity of 24.6 μS cm^{-1}, 23.1 μS cm^{-1}, 32.1 μS cm^{-1} and 41.0 μS cm^{-1}, respectively. The obtained conductivities show similar values, which may suggest that this parameter should not have a crucial influence on the deposition process of the RE-layer on the steel surface. During the deposition, the electric current was recorded in order to estimate the effectiveness of the deposition process. Based on this measurement, the electric charge per cm^2 was calculated and shown in Fig. 2A. The calculated value of deposited RE-oxide according to charge (for the deposition time of 1 min) is 3,28, 59,6; 22,9 and 19,9 μmol × C^{-1} for Ce-, Gd-, La-, and Y-oxide, respectively. According to Faraday's first law, the deposition efficiency of the proposed method was calculated for each RE-oxide. The determined efficiencies are 60%, 79%, 79%, and 80% for the deposition of Ce-, Gd-, La-, and Y-oxide, respectively. In the initial stage of the study, the dependence of the deposition time on the deposit weight was studied, and Fig. 2B shows the results. For this purpose, a series of Crofer 22 APU steel samples with different deposition times (of up to 4 min) were prepared.

The deposition of the La-coating showed the highest weight gain, thus deposition times within 10−60 s were also studied. The deposition of the La-oxide layer seems more intense than the other coatings. It was estimated, assuming formation of a continuous and dense layer, that 10 s of La-oxide deposition results in ~24 nm layer thickness (16 μg cm^{-2}), while in the case of Y-oxide deposition, 1 min of deposition results in ~37 nm layer thickness (44 μg cm^{-2}). Calculated layer thicknesses can be compared with those obtained by theoretical calculations. Namely, ~30 nm for La-oxide and ~46 nm for Y-oxide were obtained, which is
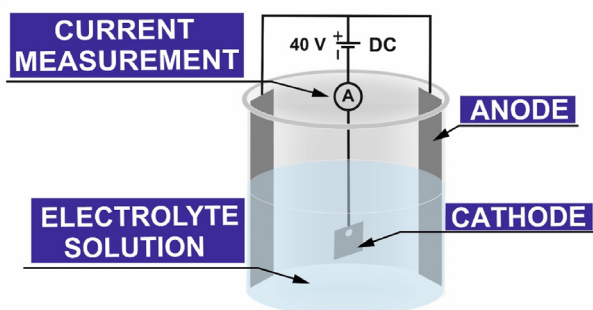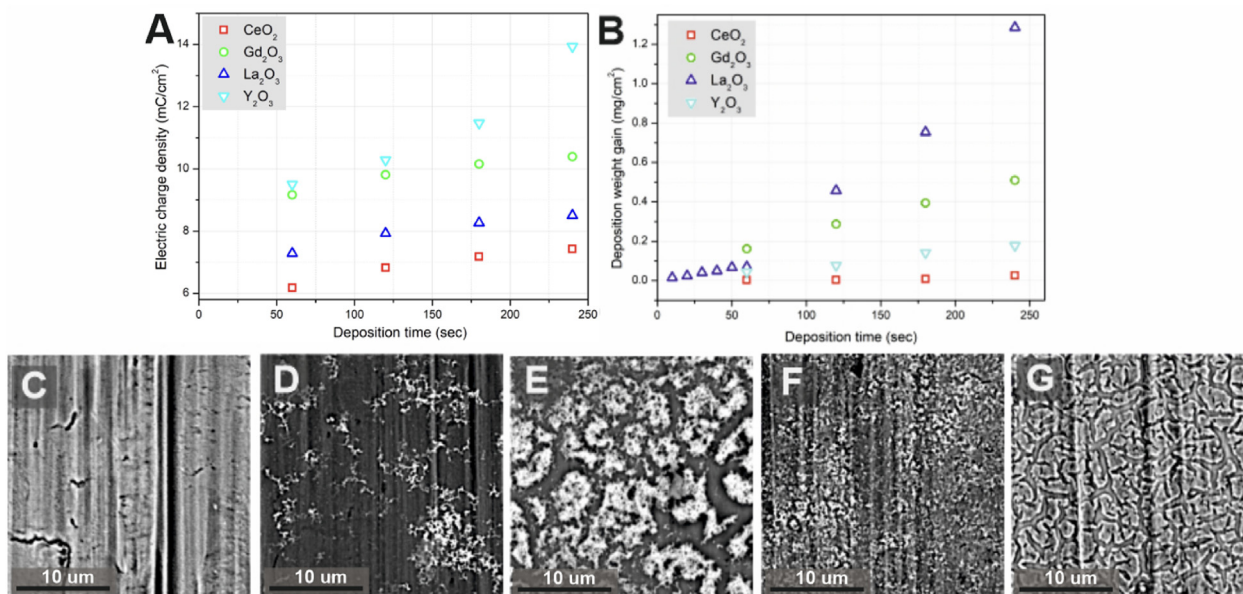

Fig. 1 − Sketch of the deposition setup.

Fig. 2 — **Electric charge density vs. the deposition time (A) weight of the coating materials vs. the deposition time (B), SEM surface images of the reference, uncoated steel (C), Ce- (D), Gd- (E), La- (F), Y- (G) coated for 1 min.**

reasonably close to the experimentally calculated layer thicknesses and at the same time to the mass change values given in Fig. 2B. Since 10 s is a relatively short time, the weight obtained during the electrodeposition process was compared with the dip coating technique. In the case of the La-oxide layer, ten times greater weight gain was obtained during 10 s of La-nitrate deposition in comparison with the dipped sample in the La-nitrate solution for the same period of time.

Electron microscopy images of the 60 s deposits are presented in Fig. 2 C–G. In nearly all cases, the deposits are visible as discontinuous layers. The presence of the respective RE was further confirmed by EDS analysis, where the RE content (based on low magnification surface analysis) was estimated to be ~1 at.% for the prepared coatings. The weight gain results show that the Ce-oxide layer is less effectively formed in comparison with the other layers. The SEM observations showed that Ce-oxide is formed as randomly distributed deposits. Local agglomerates of deposited RE-oxides are visible. However, according to the EDS analysis on the surface of steel samples (where the RE-oxide layer is not visible), the concentration of the analysed rare earth elements is in the range of 0.6–0.7% by area. In the case of the areas where these agglomerates occur, the obtained result of atomic concentration increases to 1.2%. The mapping of elements in combination with the determined deposition efficiency indicates the efficiency of the process. Formed oxide agglomerates may be caused by local imperfections of the steel surface (formed in the process of rolling steel, which can be seen in the reference sample). Despite this observation, the EDS tests clearly show the presence of deposited Ce oxides in significant amounts, though it is impossible from these measurements to judge the layer thickness or its continuity. Nevertheless, all tested RE layers were further investigated since the RE layer quality on corrosion protection effectiveness is unknown.

Short-term corrosion evaluation

Initial corrosion screening at 900 °C
After the fabrication of samples with different weights of the RE-oxide layer, the samples were subjected to high temperature oxidation to assess the influence of the oxide layer thickness on the corrosion rate. This helps the selection of samples for extended measurements.

The effect of the coating deposition time (~thickness) on the weight gain of the samples was determined by cyclic oxidation at a temperature of 900 °C for 250 h (5 cycles of 50h). An initial test at a relatively high temperature of 900 °C was carried out to highlight the differences resulting from the physicochemical properties of the oxides in a short time frame — it acts as an accelerated test procedure.

For the Ce-, Gd-, and Y-oxide layers, samples with deposition times varying between 1 min and 4 min were studied. The time was also varied between 10 and 60 s due to the formation of thick deposits.

The oxidation weight gain values for samples exposed at 900 °C are shown in Fig. 3. In all cases, the uncoated steel was used as a reference. The weight gain of the uncoated Crofer 22 APU steel after 250 h at 900 °C is ~0.6 mg cm^{-2}, which is consistent with the literature data. Talic et al. reported virtually the same value for a Crofer 22 APU sheet with a similar thickness (1 mm) [33].

The deposition of all coatings resulted in visibly reduced weight gains caused by oxidation. The obtained weight gain data indicates that there was no significant effect of the deposition time on the weight gain. The average weight gain of the coated steel sheets was similar in all cases (~0.37 mg cm^{-2}). The weight gain difference between the uncoated and coated alloys was ~40%, which is a marked improvement in corrosion resistance. Similar thermogravimetric results at high temperatures for the oxides analysed
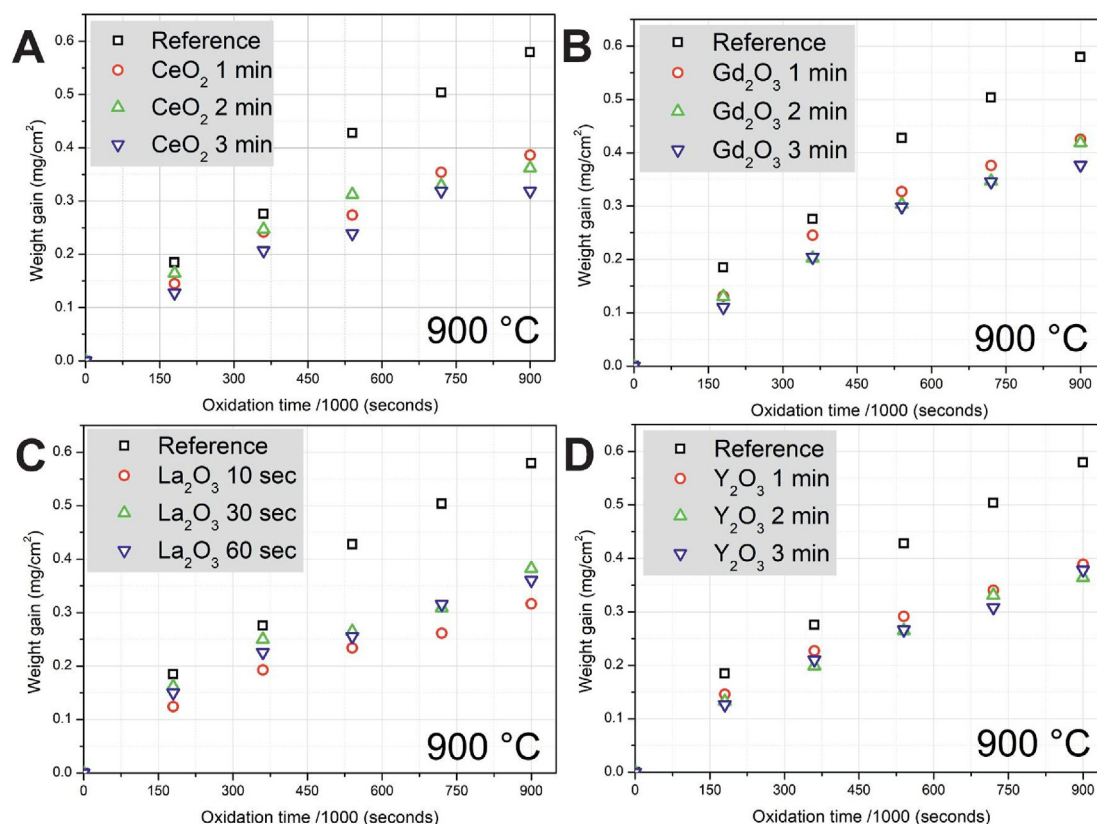
Fig. 3 — Weight gain curves for samples oxidised at 900 °C deposited with a layer of: Ce- (A), Gd- (B), La- (C), Y- (D).

may have a different basis. The fact is that even a thin layer of rare earth oxides reduces weight gain. High corrosion temperature (900 °C) affects the corrosion rate and the influence of RE-oxides is visible. Therefore, despite the lower efficiency in the deposition of cerium oxide compared to other analysed ceramics, the result is ultimately similar. The initial stage of oxidation of the cerium oxide coated sample shows the least reduction of weight gain compared to the other RE-oxide layers. This information may indicate the behaviour of cerium oxide at lower temperatures. Another observation is the flattening of the weight gain for lanthanum oxide, which initially showed similar values to the reference sample, then to slow down the oxidation process and get the most promising result. Each of the described results indicates that each of the rare earths has its own physical–chemical process behind the reduction of weight gain under the influence of oxidation.

Based on these results, the samples prepared with the shortest deposition times (10 s for La-oxide and 1 min for Ce-, Gd-, and Y-oxides) were selected for further research. These samples showed (Fig. 2 B) the deposited weights in the range of 0.01–0.05 mg cm^{-2} (60 s deposition for Ce-, Gd-, and Y-oxides, and 10 s for the La-oxide coating). Based on layer weight, one can predict the layer thickness. The theoretical average equivalent thickness of the coating is 50 nm when the density of the RE oxides (5–7 g cm^{-3}) and the specified deposit weight are considered.

Short-term corrosion exposure at 900/800/700 °C

The selected samples were tested for their corrosion properties at lower temperatures for 800 °C and 700 °C. Typically, the temperature range between 900 °C and 700 °C is most often studied for the determination of corrosion properties of alloys used in solid oxide cell stacks [34].

The weight gain results for 800 °C and 700 °C are shown in Fig. 4. At all temperatures, the uncoated samples have the largest weight gain, also confirming the protective properties of the coating materials used at lower temperatures. At 800 °C, the lowest weight gain was obtained for the Y-oxide coated sample (~0.089 mg cm^{-2}), followed closely by the Gd-oxide coated sample (~0.093 mg cm^{-2}). The La-oxide coated samples showed intermediate weight gain values, with the weight gain of the Ce-oxide samples closest to the uncoated alloy.

At 700 °C, the weight gain behaviour is similar to that observed at 800 °C. The lowest weight gain is noted for the Gd-oxide coated sample (~0.028 mg cm^{-2}), whereas the Y-oxide and La-oxide coated samples are slightly worse, but still present a lower weight gain than the uncoated sample. Again, the Ce-oxide coated alloy has a weight gain quite similar to the uncoated alloy.

Analysing the results of oxidation at 700, 800, and 900 °C, it seems that the sample with ceria layer coating is effective only at the highest temperature, whereas the Gd-oxide, La-oxide, and Y-oxide are effective in the whole temperature range. The Gd-oxide coating seems the most effective at
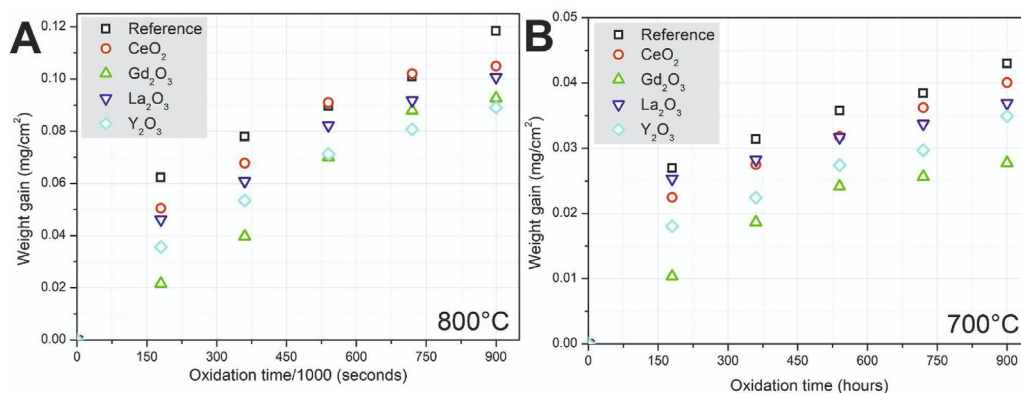
Fig. 4 — Weight gain and parabolic plots for samples oxidised (for 250 h) at 800 °C (A) and 700 °C (B).

reducing the oxide growth, especially in lower temperatures (700 °C). That confirmed the first ~100 h at 800 °C, during which the Gd_2O_3 -based layer showed less weight gain than the other ceramic layers, but in the subsequent phase of the experiment, the samples with the gadolinium oxide layer showed growing weight gain, and finally, after 150 h, they showed a higher weight gain than the sample coated with yttria. RE-oxide coatings are able to provide a marked reduction of the oxide growth rate even at a moderate temperature of 700 °C, which seems especially important since, e.g., the Mn—Co oxide spinels do not provide an oxide growth rate reduction at this temperature [30]. Thus, by potentially combining these two coating materials (RE + spinel), a synergistic low-temperature effective coating can be designed.

Electrical resistivity measurements. The weight gain measurements showed a protective effect of the applied thin coatings in terms of the lowered weight gain. The influence of the coatings can also be studied by electrical resistivity measurements. The thicker the oxide scales formed on the alloys due to oxidation, the higher the cross-scale electrical resistance of the alloys. The deposited ceramic coatings can also influence the electrical resistivity of the samples since the oxide form of the coated elements (CeO_2, Gd_2O_3, La_2O_3 and Y_2O_3) are electrical insulators. Thus, their applicability to solid oxide cell stacks should not negatively influence the electrical properties, which must be studied.

The Area Specific Resistance (ASR) was studied on samples after the 250-h oxidation test at 700, 800 and 900 °C. Graphs showing the temperature dependence of the ASR, including the comparison of the ASR values obtained at 700 °C, are shown in Fig. 5. The ASR results show that in almost all cases, the samples with the applied coatings have a lower electrical resistance than the uncoated samples (with the exception of the Ce-coated alloy oxidised at 800 °C). As indicated in Fig. 5 A—C and summarised in D, there is a strong effect of the exposure temperature on the resulting ASR level: the higher the exposure temperature, the higher the resistance. For example, for the uncoated samples, the ASR values after 250 h of exposure at 900, 800, and 700 °C were ~140 mΩ cm², ~70 mΩ cm² and ~35 mΩ cm² (values measured at 700 °C, Fig. 5 D). For the surface-modified samples, the

lowest ASR values were obtained for the yttria-coated series. The ASR values were ~95 mΩ cm², ~15 mΩ cm² and ~7 mΩ cm² after 250 h exposures at 900/800 and 700 °C. The difference in the ASR between the uncoated and the Y-oxide coated sample is pronounced at lower oxidation temperatures, where as high as a 5-fold decrease in the ASR value was obtained. For the Ce-oxide, Gd-oxide, and La-oxide modified samples, the ASR values were also lower than for the reference sample (except for the ceria coated sample measured at 800 °C), with the Gd-oxide and La-oxide coatings being slightly inferior to the Y-oxide coating. The slopes of the ASR curves were also similar for all samples, indicating a similar overall conductivity mechanism of the uncoated and coated samples, most probably dominated by chromia scale in all cases.

The RE coating procedure, especially in the case of Y-oxide and La-oxide, has a very positive effect on the resulting ASR value, which is very important for efficient and low-degradation SOC stacks.

After short-term weight gain and ASR measurements, the samples were analysed by scanning electron microscopy (SEM). Micrographs of the sample cross-sections were taken to assess the differences in the surface structure after short-term corrosion at 700 °C, 800 °C and 900 °C. Selected images of the lanthanum coated samples are shown in Fig. 6.

At 700 °C, where the weight gain was very low (~0.035 mg cm⁻²), only a very thin, rough corrosion layer is visible. No sign of the La-oxide coating is noticeable. At 800 °C, due to the higher weight gain (~0.1 mg cm⁻²), the oxide layer becomes more apparent. The formed oxide uniformly covers the sample surface. Within the oxide (in the middle), a very thin bright layer is visible, which is the deposited La-oxide material. The sample at 900 °C has the highest weight gain (~0.35 mg cm⁻²) and traces of the La-oxide coating are noticeable on the surface of the oxide.

Long-term oxidation at 700 °C

A temperature of 700 °C was selected for performing the longer-term study, as it is of interest for intermediate temperature SOFC technology [35]. As discussed, the RE-oxide coatings seem to provide an important reduction in oxide scale growth at this temperature. The exposures were
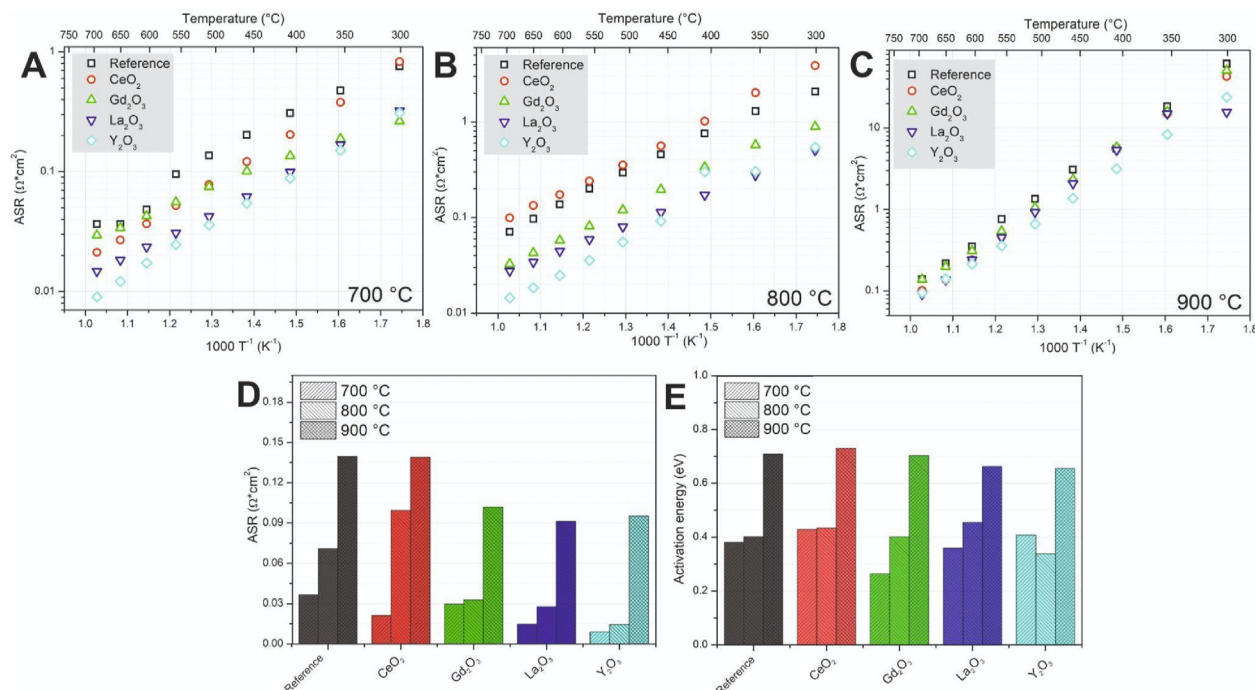
Fig. 5 – Arrhenius plots of Area Specific Resistance of samples oxidised at 700 °C (A), 800 °C (B) and 900 °C (C) for 250 h, and a comparison of ASR values measured at 700 °C (D) and comparison of the activation energies (E).
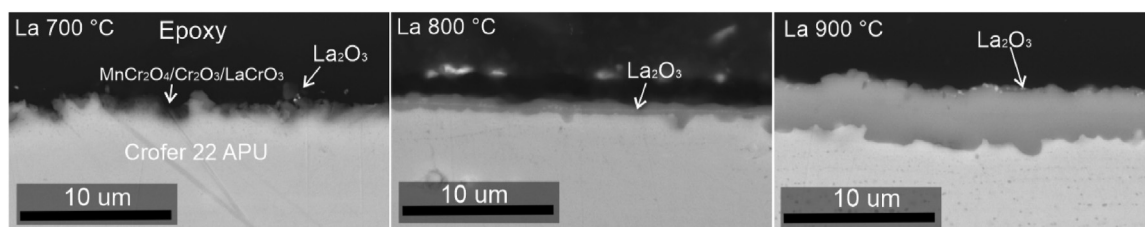

Fig. 6 – SEM pictures of the cross-section for La-coated samples. From the left for 700 °C, 800 °C and 900 °C.

performed up to 2000 h (8 cycles of 250 h) and the obtained weight gain results are presented in Fig. 7 A together with a parabolic plot (Fig. 7 B).

Typically, the weight gain values determined at 700 °C are very low due to slow corrosion kinetics [19]. The weight gain was again the highest for the uncoated alloy; after 2000 h it reached ~0.09 mg cm^{-2}. The coated samples showed lower weight gain values, with the yttria- and La-oxide coated alloys resulting in a weight gain of ~0.055 mg cm^{-2}, so a decrease of ~40% was achieved.
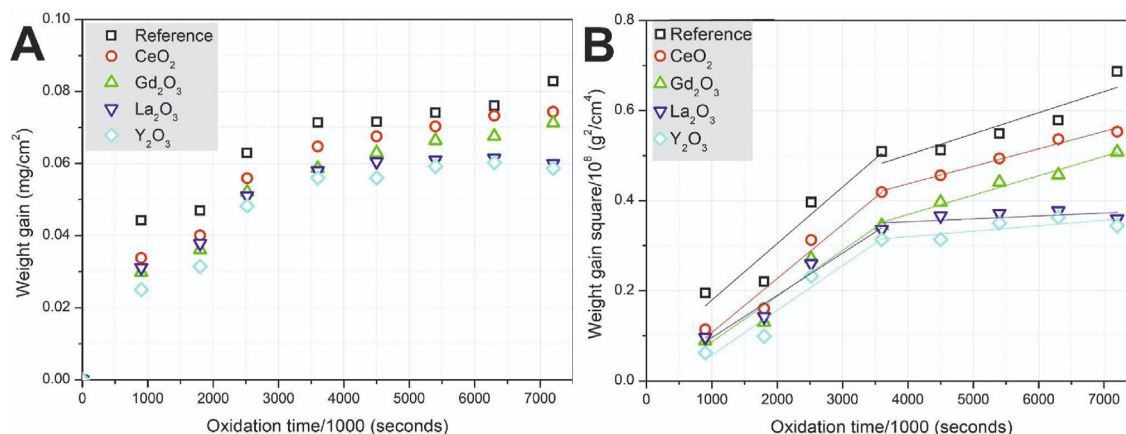

Fig. 7 – Weight gain (A) and parabolic plot (B) for the long-term oxidation of differently coated samples at 700 °C (A, B).

When considering the kinetics of high-temperature oxidation, usually a square (parabolic) dependence of the weight increase vs. time is used:

$$\left(\frac{\Delta m}{A}\right)^2 = k_p t + C$$

where: Δm is the weight gain [g], A is the sample area [cm^2], k_p is the corrosion rate parameter [g^2 cm^{-4} s^{-1}], t is the oxidation time [s], and C is the integration constant [g^2 cm^{-4}].

A parabolic plot of the weight gain values is presented in Fig. 7B. Due to its nonlinear behaviour, the fitting of the k_p was performed separately for the periods of 250–1000 and 1000–2000 h. The calculated k_p values are summarised in Table 1. The constant C is usually assigned to the initial corrosion phenomena. For the uncoated samples, the C value is visibly larger than for the coated alloys, meaning that the initial stage of corrosion was modified by the addition of the reactive element.

The initial oxidation of the alloys follows a similar kinetics, where the k_p values range from 1.26 x10^{-15} g^2 cm^{-4} s^{-1} to 0.94 x10^{-15} g^2 cm^{-4} s^{-1} for the uncoated and La-oxide coated alloys, respectively. A more pronounced difference is visible for the 2nd analysis period (1000–2000 h), where the corrosion kinetics slows down. The difference between the uncoated and the La-oxide coated sample is one order of magnitude. Also, the Y-oxide coated sample shows a marked corrosion rate decrease. The samples coated with Gd-oxide and Ce-oxide show little improvement.

The possible change of slopes of the weight gain is often reported in the literature. One of the reasons might be changes in the chemistry of the layers, including phase stabilisation/grain growth (e.g., Cr$_2$O$_3$ and/or (Mn,Cr)$_3$O$_4$), or depletion of oxide scale-forming elements (Mn) from the substrate. Additionally, differences in the formation of spinel (Mn,Cr)$_3$O$_4$ and chromium oxide may be caused by the formation of protective phases during the conversion of deposited Ce-/Gd-/La-/Y-oxide coating precursors [36].

Overall, the deposited reactive element coatings, especially in the case of the Y$_2$O$_3$ and La$_2$O$_3$ coatings, resulted in a marked improvement in corrosion resistance.

After the long-term exposure test, the samples were also subjected to electrical resistivity measurements. The results are shown in Fig. 8. The samples coated with La-, Gd-, and Y-oxide show a visible decrease of the ASR, whereas Ce-oxide has a minor effect. The highest ASR values at 700 °C were found for the uncoated samples (~85 mΩ cm^2 at 700 °C). Slightly lower values were found for the Ce-, Y- and La-oxide coated samples (~45 mΩ cm^2 for Ce-oxide, ~35 mΩ cm^2 for

yttria and La-oxide). The lowest ASR value was obtained for the Gd-oxide modified sample (~20 mΩ cm^2). At a temperature of <600 °C, the highest resistance was obtained for the ceria-coated sample, which showed an activation energy of ~0.55 eV.

The ceria-coated sample showed the highest ASR, possibly due to the combination of several effects. The first is the ceria layer itself, which is an electrical insulator, and the weight gain of the Ce-oxide coated sample was comparable to that of the reference, uncoated sample (especially at lower temperatures). This contributes to the formation of a fairly thick corrosion layer on top of which the cerium oxide layer is deposited. Ultimately, this increases the ASR value even compared to the reference sample. Also, the slope of the obtained curve clearly indicates the highest activation energy. The La-oxide and Y-oxide coated samples showed improvement compared to the reference sample. Despite the thicker layers, the ASR values were lower due to the formation of a much thinner corrosion layer for the La-oxide-based layer. In the case of the Y-oxide based layer, this value was slightly worse because the layer itself was the most continuous of all. This was also confirmed by the activation energy values. The best ASR properties were obtained for samples coated with Gd-oxide. The thickest layer of the Gd$_2$O$_3$-based sample did not cause the thinnest corrosion layer, but even this did not prevent the greatest decrease in the ASR value. The application of Gd-oxide-based coating led to a 4-fold decrease in the ASR, which is an important achievement regarding potential long-term stack operation.

In Fig. 9 A X-ray diffractometry analysis was performed on the samples oxidised at 700 °C for 2000 h. Due to the small thickness of the oxide coating layer, the intensity of the coatings-related peaks is low but still allows qualitative identification.

For the uncoated sample, the peaks from the steel substrate could be detected together with the peaks from the formed oxide phases. The most intensive peak came from the cubic MnCr$_2$O$_4$ (ICDD card #75–1614) followed by Cr$_2$O$_3$ (#38–1479). The measured peaks were shifted in comparison to the database inputs, but qualitatively they very well describe the oxides. The shift might be caused by sample misalignment or a slight difference in the chemical composition of the oxides. The two found oxide phases are typical for Crofer 22 APU oxidised in the conditions used [36,37].

The analysis of the coated samples revealed some differences in the oxide scale formation on different substrates. The sample coated with cerium showed the formation of (MnCr)$_3$O$_4$, Cr$_2$O$_3$ and the CeO$_2$ phase (#34–394), which seems

Table 1 – Determined values of the k_p coefficient corresponding to the kinetics of the oxidation reaction. Corrosion was divided into two stages (1st from 250 to 1000 h, 2nd from 1000 h to 2000 h) due to the visible difference in the reaction rate.

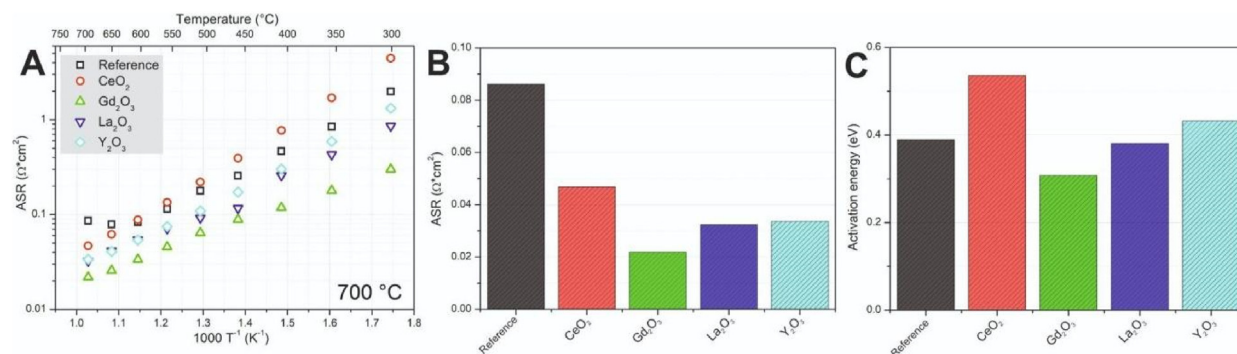| Temperature	$k_{p\ (250h–1000h)}$ [x 10^{-15} g^2 cm^{-4} s^{-1}]	C [x 10^{-10} g^2 cm^{-4}]	$k_{p\ (1000h–2000h)}$ [x 10^{-15} g^2 cm^{-4} s^{-1}]	C [x 10^{-9} g^2 cm^{-4}]
Reference	1.26	5.35	0.47	3.41
CeO$_2$	1.20	1.25	0.39	2.82
Gd$_2$O$_3$	1.01	1.15	0.43	1.97
La$_2$O$_3$	0.94	0.21	0.07	3.27
Y$_2$O$_3$	1.00	4.26	0.12	2.71

Fig. 8 – Arrhenius plots of Area Specific Resistance of samples oxidised at 700 °C for 2000 h (A), comparison of ASR values measured at 700 °C (B) and comparison of the activation energies (C).
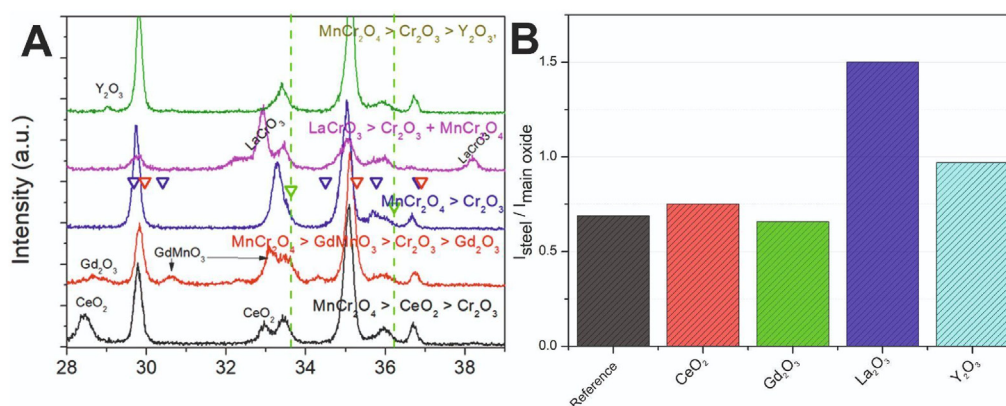

Fig. 9 – XRD spectra of coated alloys after 2000 h of oxidation (A), relative ratio of the intensities of the steel peak to the main peak of the oxide phase (B).

to retain its fluorite structure. In the case of the gadolinium-coated sample, the most intensive peaks came from the $MnCr_2O_4$ spinel, followed by $GdMnO_3$ (#25–337), Cr_2O_3 and Gd_2O_3 (#12–797) phases. Gadolinium oxide reacts with manganese oxide, forming a new phase. Some gadolinium remained in the pure oxide form. The La-oxide coated sample showed the formation of a $LaCrO_3$ perovskite phase (#24–1016), which was the most intense peak. In addition, Cr_2O_3 could be detected. For this sample, the formation of the $MnCr_2O_4$ seemed suppressed – it had the lowest relative intensity among the studied samples. In the case of the samples with a Y_2O_3 layer, the most intense peak corresponded to cubic $MnCr_2O_4$. The less intense peak corresponded to Cr_2O_3 and the least intense, but still characteristic peak, to Y_2O_3 (# 41–1105) [38–41].

To qualitatively compare the oxide scale thickness formed on different samples, the relative intensity ratio of the main steel substrate peak and the most intensive oxide phase peaks is plotted in Fig. 9 B.

For the long-term samples, the sample with the La-based layer had the highest value of the intensity ratio coefficient. This was mainly due to the formation of the chromium-lanthanum spinel. This spinel is the most intense peak in the diffraction pattern. There is no visible spinel in the Y_2O_3 layer, only the oxide itself. These two layers also showed the lowest weight gain. In the case of the sample with a layer of

cerium oxide and gadolinium oxide, both the presence of the oxide and the spinel were identified. At the same time, these samples showed a little better weight gain properties than the reference sample.

The results obtained are supported by studies conducted by Chevalier et al. [40]. In his work, he investigated the formation of perovskites from Gd-oxide, Y-oxide and La-oxide. The tests were performed at a temperature of 1000 °C. Chevalier showed that La_2O_3 converts to perovskites very quickly. Gd_2O_3 transforms much slower (more than 100 h at this high temperature). In the case of Y_2O_3, this time was even longer, nearly 300 h. In our case, the described tests were carried out at a lower temperature (700 °C) but the phase formation after 2000 h of exposure was similar [42]. Gil et al. undertook the task of explaining the effect of the grain structure on the oxidation product in the case of the application of protective layers on steel. Studies have shown that thin yttria layers do not form a continuous layer at temperatures close to 1000 °C. At lower temperatures, the oxide forms a continuous layer. However, attention should be paid to the short measurement time of 100 h. When using longer times, a tendency towards oxide discontinuity may be observed. The formation of perovskite in the form of $YCrO_3$ facilitates the slow diffusion of oxygen to the inside, which at the same time significantly slows down the diffusion of chromium to the outside [37]. The cited studies show that the temperature of

700 °C is too low for the formation of the perovskite form of $YCrO_3$. More time and a higher temperature are needed to produce such a phase that could inhibit the diffusion of chromium to the outside. This problem does not occur in the case of lanthanum, which is produced in a significant amount in the form of $LaCrO_3$, and even the shorter deposition time

and the thinner layer did not significantly deteriorate the thermogravimetric results obtained. The samples with Gd2O3 and CeO2 partially form a perovskite phase, so the protective effect is more complex. It seems that several "protective" mechanisms are plausible, and these have been studied for many years, as pointed out in a recent summary of Chevalier
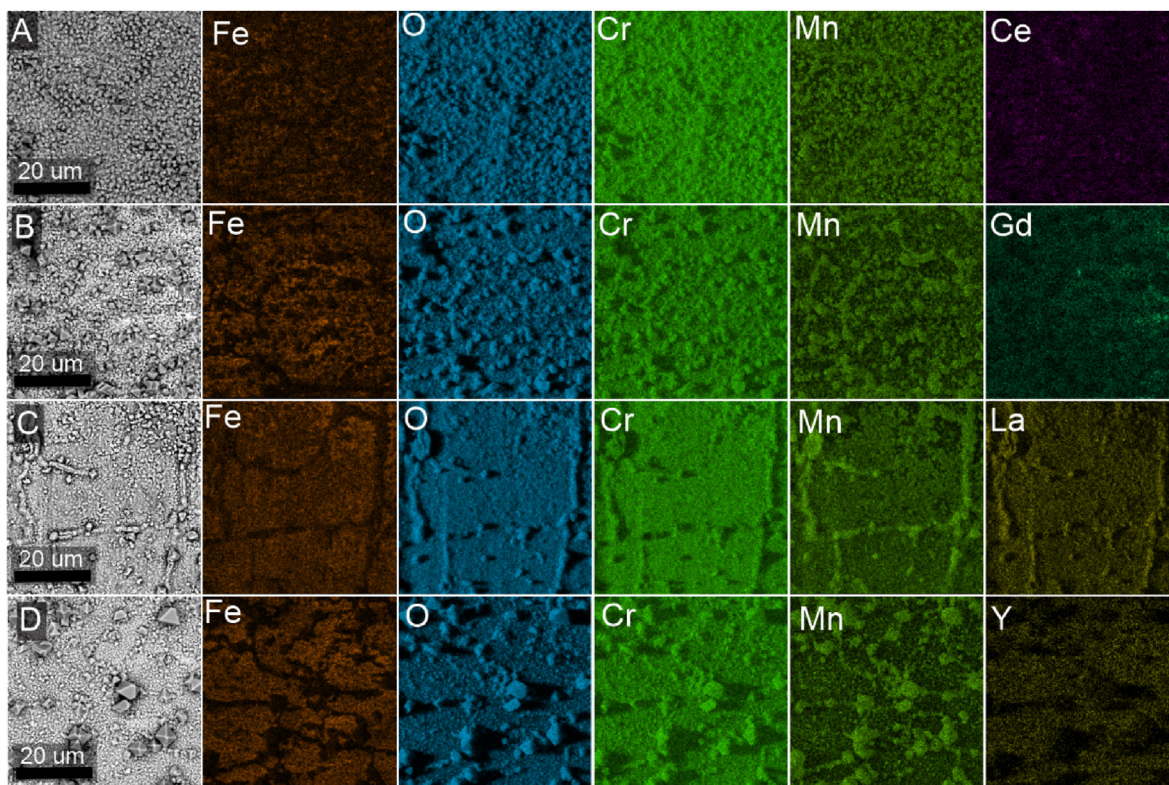

Fig. 10 — SEM and EDS elemental maps of surfaces of CeO_2 (A), Gd_2O_3 (B), La_2O_3 (C) and Y_2O_3 coated (D) samples after 2000 h of oxidation at 700 °C.
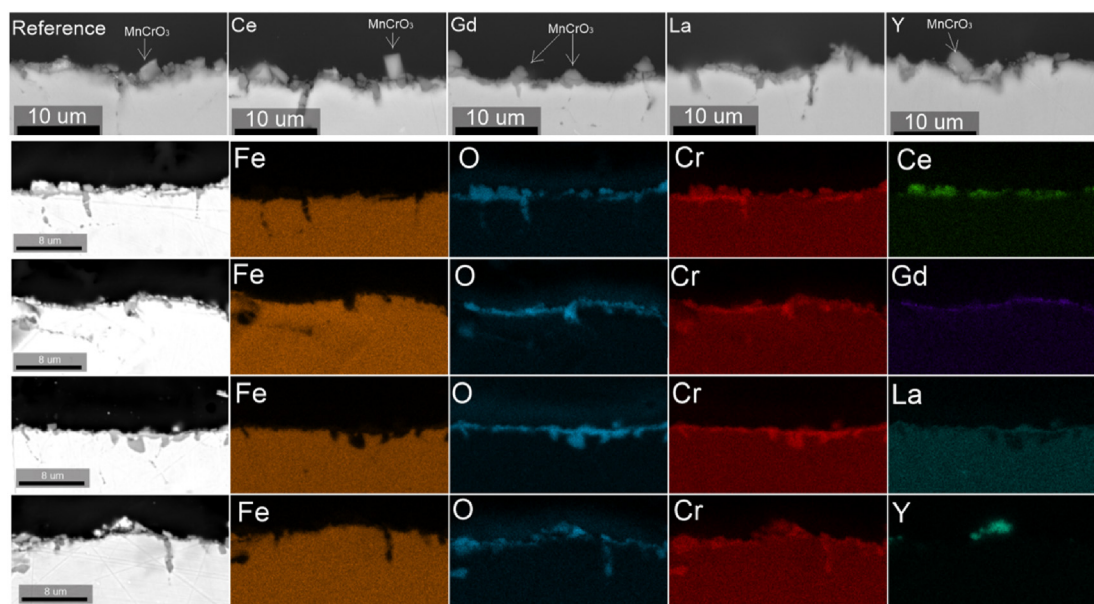

Fig. 11 — SEM photos and the EDS analysis taken for sections of samples after long-term corrosion at 700 °C for the discussed layers and the reference sample.

[43]. Nevertheless, both thermogravimetric, electrical and XRD measurements show the importance and effectiveness of rare earths in corrosion protection.

A post-mortem examination was performed by SEM/EDS to analyse the surfaces and cross-sections of the samples. This analysis was performed after 2000 h at 700 °C. The results are shown in Fig. 10 and Fig. 11.

On the Ce-oxide and Gd-oxide coated samples' surfaces, small (1−2 μm) manganese-chromium spinel crystals are visible. The Y-oxide coated sample shows the largest surface crystallites, which are composed of Cr and Mn. In these cases, the active elements seem to be distributed uniformly on the surface of the alloy and are not present in the large crystallites.

The samples based on a layer of La_2O_3 show a different surface morphology. In this case, it seems that the formation of the $LaCrO_3$ perovskite phase occurred uniformly over the sample surface. According to the XRD, this indicates a significantly reduced formation of $MnCr_2O_4$, which seems to grow along the alloy grain boundaries. The surface of the La-oxide coated sample is the smoothest, with no large crystallites.

The results of the SEM/EDS cross-section analyses are presented in Fig. 11. The oxidation at 700 °C resulted in a very thin oxide scale. The corrosion products seem similar in all cases. The chemical composition of the outer oxide determined by EDS shows the presence of reactive elements at some spots. The coatings are not continuous as they are quite thin and they react with the Mn/Cr oxide scale. Some internal oxidation is visible on all samples, which is connected to the growth of the oxide scale in the grain boundaries of the alloy.

Conclusions

This article presents the results of the electrodeposition of Ce-, Gd-, La-, and Y-oxide coatings based on ethanol solutions of dissolved reactive element nitrates. In terms of reducing the kinetics of oxide scale growth, all of the coatings performed similarly. This was confirmed by both thermogravimetric and electrical resistivity measurements. The lowest weight gain was obtained for the Y-oxide and La-oxide based coatings, where the corrosion rate parameter was decreased by ~40%. The electrical resistivity of the oxide scale was reduced by a factor of 4-7-fold depending on the particular coating. X-ray diffractometry allowed for the qualitative identification of the oxides on the surface of the Crofer 22 APU plates. The reactive elements showed different reactivity with the Mn/Cr from the alloy. In the case of the yttria coated sample, no reaction with Cr/Mn was detected, whereas for the La-oxide coated samples, transformation of the La-oxide coating to $LaCrO_3$ perovskite was apparent. SEM microscopy confirmed the dissimilar behaviour of the different coatings. In the case of the La-oxide coating, its distribution was also uniform on the sample surface and no large Mn−Cr oxide spinel particles were formed, whereas in the case of the Y-oxide coating, its distribution was also uniform but large Mn−Cr oxide crystallites grew. Overall, the most promising layers seem to be either La-/Y-/Gd-oxide based, offering quite similar performance and benefits.

Declaration of competing interest

The authors declare that they have no known competing financial interests or personal relationships that could have appeared to influence the work reported in this paper.

REFERENCES

[1] Niewolak L, Wessel E, Singheiser L, Quadakkers WJ. Potential suitability of ferritic and austenitic steels as interconnect materials for solid oxide fuel cells operating at 600 °C. J Power Sources 2010;195:7600−8. https://doi.org/10.1016/J.JPOWSOUR.2010.06.007.

[2] Reisert, M.; Aphale, A.; Singh, P. Materials solid oxide electrochemical systems: Material degradation processes and novel Mitigation Approaches., doi:10.3390/ma11112169.

[3] Ghiara, G.; Piccardo, P.; Bongiorno, V.; Geipel, C.; Spotorno, R. Characterization of metallic interconnects extracted from solid oxide fuel cell stacks operated up to 20,000 h in real life conditions: The Air Side., doi:10.3390/en13246487.

[4] Mah JCW, Muchtar A, Somalu MR, Ghazali MJ. Metallic interconnects for solid oxide fuel cell: a review on protective coating and deposition techniques. Int J Hydrogen Energy 2017;42:9219−29. https://doi.org/10.1016/J.IJHYDENE.2016.03.195.

[5] Zhu WZ, Deevi SC. Development of interconnect materials for solid oxide fuel cells. Mater Sci Eng, A 2003;348:227−43. https://doi.org/10.1016/S0921-5093(02)00736-0.

[6] Fontana S, Chevalier ● S, Caboche ● G, Lamour J, Chevalier S, Caboche ÁG, Caboche G. Metallic interconnects for solid oxide fuel cell: performance of reactive element oxide coating during 10, 20 and 30 Months exposure made of La 2 O 3 or Y 2 O 3 resulted in an important improvement in the high. Oxid Met 2012;78:307−28. https://doi.org/10.1007/s11085-012-9308-4.

[7] Brylewski T, Kucza W, Adamczyk A, Kruk A, Stygar M, Bobruk M, Dabrowa J. Microstructure and electrical properties of Mn1+xCo2−xO4 (0≤x≤1.5) spinels synthesized using EDTA-gel processes. Ceram Int 2014;40:13873−82. https://doi.org/10.1016/J.CERAMINT.2014.05.106.

[8] Brylewski T, Kruk A, Bobruk M, Adamczyk A, Partyka J, Rutkowski P. Structure and electrical properties of Cu-doped Mn-Co-O spinel prepared via soft chemistry and its application in intermediate-temperature solid oxide fuel cell interconnects. J Power Sources 2016;333:145−55. https://doi.org/10.1016/J.JPOWSOUR.2016.09.136.

[9] Bobruk M, Brylewska K, Durczak K, Wojciechowski K, Adamczyk A, Brylewski T. Synthesis of manganese-cobalt spinel via wet chemistry methods and its properties. Ceram Int 2017;43:15597−609. https://doi.org/10.1016/J.CERAMINT.2017.08.116.

[10] Kruk A, Stygar M, Brylewski T. Mn-Co spinel protective-conductive coating on AL453 ferritic stainless steel for IT-SOFC interconnect applications. J Solid State Electrochem 2013;17:993−1003. https://doi.org/10.1007/s10008-012-1952-8.

[11] Szymczewska D, Molin S, Chen M, Ski PJ, Hendriksen PV. Corrosion study of ceria protective layer deposited by spray pyrolysis on steel interconnects. Ceram Eng Sci Proc 2017;37:79–86. https://doi.org/10.1002/9781119320197.ch7.

[12] Szymczewska D, Molin S, Vang Hendriksen P, Jasí Nski P. Microstructure and electrical properties of Fe,Cu substituted (Co,Mn) 3 O 4 thin films. 2017. https://doi.org/10.3390/cryst7070185.

[13] Cabouro G, Caboche G, Chevalier S, Piccardo P. Opportunity of metallic interconnects for ITSOFC: reactivity and electrical property. J Power Sources 2006;156:39–44. https://doi.org/10.1016/J.JPOWSOUR.2005.08.039.

[14] Piccardo P, Gannon P, Chevalier S, Viviani M, Barbucci A, Caboche G, Amendola R, Fontana S. ASR evaluation of different kinds of coatings on a ferritic stainless steel as SOFC interconnects. Surf Coating Technol 2007;202:1221–5. https://doi.org/10.1016/J.SURFCOAT.2007.07.096.

[15] Grolig JG, Froitzheim J, Svensson JE. Effect of cerium on the electrical properties of a cobalt conversion coating for solid oxide fuel cell interconnects − a study using impedance spectroscopy. Electrochim Acta 2015;184:301–7. https://doi.org/10.1016/J.ELECTACTA.2015.10.111.

[16] Molin S, Kusz B, Gazda M, Jasinski P. Evaluation of porous 430L stainless steel for SOFC operation at intermediate temperatures. J Power Sources 2008;181:31–7. https://doi.org/10.1016/J.JPOWSOUR.2007.10.009.

[17] Ebrahimifar, H.; Zandrahimi, M. Oxidation and electrical behavior of a ferritic stainless steel with a Mn-Co-based coating for SOFC interconnect applications., doi:10.1007/s11085-015-9557-0.

[18] Gannon PE, Tripp CT, Knospe AK, Ramana CV, Deibert M, Smith RJ, Gorokhovsky VI, Shutthanandan V, Gelles D. High-temperature oxidation resistance and surface electrical conductivity of stainless steels with filtered arc Cr−Al−N multilayer and/or superlattice coatings. Surf Coating Technol 2004;188–189:55–61. https://doi.org/10.1016/J.SURFCOAT.2004.08.067.

[19] Canovic S, Froitzheim J, Sachitanand R, Nikumaa M, Halvarsson M, Johansson LG, Svensson JE. Oxidation of Co- and Ce-nanocoated FeCr steels: a microstructural investigation. Surf Coating Technol 2013;215:62–74. https://doi.org/10.1016/J.SURFCOAT.2012.08.096.

[20] Falk-Windisch H, Claquesin J, Sattari M, Svensson JE, Froitzheim J. Co- and Ce/Co-coated ferritic stainless steel as interconnect material for intermediate temperature solid oxide fuel cells. J Power Sources 2017;343:1–10. https://doi.org/10.1016/J.JPOWSOUR.2017.01.045.

[21] Magrasó A, Falk-Windisch H, Froitzheim J, Svensson JE, Haugsrud R. Reduced long term electrical resistance in Ce/Co-coated ferritic stainless steel for solid oxide fuel cell metallic interconnects. Int J Hydrogen Energy 2015;40:8579–85. https://doi.org/10.1016/J.IJHYDENE.2015.04.147.

[22] Molin S, Persson H, Skafte TL, Smitshuysen AL, Jensen SH, Andersen KB, Xu H, Chen M, Hendriksen PV. Effective yttrium based coating for steel interconnects of solid oxide cells: corrosion evaluation in steam-hydrogen atmosphere. J Power Sources 2019;440. https://doi.org/10.1016/j.jpowsour.2019.226814.

[23] Boccaccini AR, Zhitomirsky I. Application of electrophoretic and electrolytic deposition techniques in ceramics processing. Curr Opin Solid State Mater Sci 2002;6:251–60. https://doi.org/10.1016/S1359-0286(02)00080-3.

[24] Zhitomirsky I, Petric A. Electrochemical deposition of yttrium oxide. J Mater Chem 2000;10:1215–8. https://doi.org/10.1039/b000311p.

[25] Zhitomirsky I, Petric A. Electrolytic and electrophoretic deposition of CeO2 films. Mater Lett 1999;40:263–8. https://doi.org/10.1016/S0167-577X(99)00087-7.

[26] Yang L, Pang X, Fox-Rabinovich G, Veldhuis S, Zhitomirsky I. Electrodeposition of cerium oxide films and composites. Surf Coating Technol 2011;206:1–7. https://doi.org/10.1016/j.surfcoat.2011.06.029.

[27] Mazur Ł, Pleśniak J, Dąbek J, Gil A, Brylewski T. High-temperature oxidation of ferritic steel surface-modified with gadolinium oxide nanoparticles. Ceramic Materials 2019;71:179–92.

[28] Yoon JS, Lee J, Hwang HJ, Whang CM, Moon JW, Kim DH. Lanthanum oxide-coated stainless steel for bipolar plates in solid oxide fuel cells (SOFCs). J Power Sources 2008;181:281–6. https://doi.org/10.1016/J.JPOWSOUR.2007.12.053.

[29] Saeidpour F, Zandrahimi M, Ebrahimifar H. Evaluation of pulse electroplated cobalt/yttrium oxide composite coating on the crofer 22 APU stainless steel interconnect. Int J Hydrogen Energy 2019;44:3157–69. https://doi.org/10.1016/J.IJHYDENE.2018.12.062.

[30] Hamlaoui Y, Pedraza F, Remazeilles C, Cohendoz S, Rébéré C, Tifouti L, Creus J. Cathodic electrodeposition of cerium-based oxides on carbon steel from concentrated cerium nitrate solutions: Part I. Electrochemical and analytical characterisation. Mater Chem Phys 2009;113:650–7. https://doi.org/10.1016/J.MATCHEMPHYS.2008.08.027.

[31] Strydom CA, Van Vuuren CPJ. The thermal decomposition of lanthanum(III), praseodymium(III) and europium(III) nitrates. Thermochim Acta 1988;124:277–83. https://doi.org/10.1016/0040-6031(88)87030-8.

[32] Strydom CA, Vuuren CPJ, Van THE. Thermal decomposition of cerium (ill) nitrate 1987;32:157–60.

[33] Talic B, Molin S, Wiik K, Hendriksen PV, Lein HL. Comparison of iron and copper doped manganese cobalt spinel oxides as protective coatings for solid oxide fuel cell interconnects. J Power Sources 2017;372:145–56. https://doi.org/10.1016/J.JPOWSOUR.2017.10.060.

[34] Fergus JW. Synergism in the design of interconnect alloy−coating combinations solid for oxide fuel cells. Scripta Mater 2011;65:73–7. https://doi.org/10.1016/J.SCRIPTAMAT.2010.09.020.

[35] Jacobson AJ. Materials for solid oxide fuel cells. Chem Mater 2010;22:660–74. https://doi.org/10.1021/cm902640j.

[36] Molin S, Chen M, Hendriksen PV. Oxidation study of coated crofer 22 APU steel in dry oxygen. J Power Sources 2014;251:488–95. https://doi.org/10.1016/J.JPOWSOUR.2013.09.100.

[37] Gil A, Kryshtal O, Brylewski T, Czyrska-Filemonowicz A. Characterization of a Cr2O3 scale formed on chromium with implanted yttrium ions by advanced electron microscopy. Surf Coating Technol 2019;368:232–42. https://doi.org/10.1016/j.surfcoat.2019.03.081.

[38] Faisal M, Khasim S. Electrical conductivity, dielectric behavior and emi shielding effectiveness of polyaniline-yttrium oxide composites. Bull Kor Chem Soc 2013;34:99–106. https://doi.org/10.5012/bkcs.2013.34.1.99.

[39] Ma R, Jahurul Islam M, Amaranatha Reddy D, Kim TK. Transformation of CeO2 into a mixed phase CeO2/Ce2O3 nanohybrid by liquid phase pulsed laser ablation for enhanced photocatalytic activity through Z-scheme pattern. Ceram Int 2016;42:18495–502. https://doi.org/10.1016/j.ceramint.2016.08.186.

[40] Kabir H, Nandyala SH, Rahman MM, Kabir MA, Stamboulis A. Influence of calcination on the sol−gel synthesis of lanthanum oxide nanoparticles. Appl Phys Mater Sci Process 2018;124:0. https://doi.org/10.1007/s00339-018-2246-5.

[41] Tóthová E, Tarasenko R, Tkáč V, Orendáč M, Hegedüs M, Danková Z, Holub M, Baláž M, Matik M. Microcrystalline Gd 2 MoO 6 prepared by combined mechanochemical/thermal

process and its magnetic properties. J Mater Sci 2019;54:6111–21. https://doi.org/10.1007/s10853-019-03331-z.

[42] Chevalier S, Larpin JP. formation of perovskite type phases during the high temperature oxidation of stainless steels coated with reactive element oxides. Acta Mater 2002;50:3107–16. https://doi.org/10.1016/s1359-6454(02)00106-4.

[43] Chevalier S. What did we learn on the reactive element effect in chromia scale since pfeil 's patent? Mater Corros 2014;65:109–15. https://doi.org/10.1002/maco.201307310.